

Long-term evolution of the $H\alpha$ emission line of Pleione between Jan 2009 and Mar 2023 in the BeSS database

Junichi Katahira^{1*}

¹Sakai-city, Osaka 591-8021, Japan

*atak@db3.so-net.ne.jp

(Received 2023 September 29; accepted 2023 November 10)

Abstract

Using the $H\alpha$ double peak emission lines of Pleione in the BeSS database from January 2009 to March 2023, we have measured the characteristic three point intensities of the line: the intensities at the blue and red emission peaks, and the intensity of the central minimum between the peaks, and calculated the radial velocities of these three points. These values are shown over a period of 14 years. The long-term variations shown are interpreted to be split into (a) the short-term variations when the companion of Pleione is close to periastron, and (b) the long-term variations in the background. For the (b) variation, we try to explain the trajectory of the central minimum intensity by the disk precession, and discuss the occurrence of the V/R phenomenon.

Key words: stars: Be star — stars: Pleione — stars: Be disk

1. Introduction

Pleione (28 Tau, BU Tau, HD23862) is a bright member of the Pleiades cluster, with a magnitude of $V = 5.09$ (SIMBAD) and a spectral type of B8Vne (Taranova et al. 2008), and started in December 2005 the third cycle of disk formation activity with a period of about 35 years (Tanaka et al. 2007), which currently lasts until October 2023. Each disk-forming activity begins with a rapid decrease in stellar magnitude $\Delta V \sim 0.5$ mag, and exhibits spectral phase changes from the Be phase to the Be-shell phase. During a disk-formation activity, the respective periods for the Be-shell and the Be phases are curiously separated by 17 years apart (Hirata 1995). Pleione has a double peaked emission profile of $H\alpha$, and during the Be-shell phase, shows a deep shell absorption with a minimum below the continuous light level. Only a few Be stars show such a deep shell absorption. Pleione is also characterised by a periodic variation in the intensity ratio V/R of the blue and red emission peaks during the disk formation activity period (Okazaki 1997; Hirata 2007).

Pleione was detected as a speckle binary (McAlister et al. 1989), and Gies et al. (1990) confirmed its companion during the lunar occultation of Pleione. Subsequent observations using adaptive optics have detected more distant companions (Roberts et al. 2007). A hypothesis has been proposed that the speckle companion approaches the host star on a 34-year cycle, causing a disk-forming activity period (Gies et al. 1990), but it appears that the analysis of the orbital elements of the speckle companion has not progressed easily. On the other hand, the analysis of the orbital motion at the radial velocity indicated by the disk absorption line and the $H\alpha$ emission line wing preceded this speckle analysis, and it was clarified that Pleione is a single-lined spectroscopic binary star with an orbital motion

period of 218 days and an eccentricity $e = 0.6 - 0.7$ (Katahira et al. 1996; Nemravova et al. 2010). Thus, Pleione is currently considered to be at least a quadruple binary.

Since the early 2000s, a group of European amateur spectroscopic observers has published the middle-dispersion spectra of Pleione with high temporal resolution in the BeSS database¹. Pollmann and Vollmann (2014) showed that each of the three periastron passes of the companion is accompanied by drastic variations in the $H\alpha$ profile (such as large fluctuations in the V/R). These observations have visualised the interaction between the disk and the companion in a single-lined spectroscopic binary system with high eccentricity (hereafter referred to as the periastron phenomenon).

This article reports on the *re-measurement* of the attractive observational data of Pleione in the BeSS database. In section 2, we describe the data selection from the BeSS database. In section 3, we explain the data processing and the measurement method of the $H\alpha$ profile, and show the long-term variations for the intensities at the blue and red emission peaks (I_B , I_R) and at the central minimum (I_C) between the peaks, and for the radial velocities calculated at the above three points. We separate the long-term variation into the short-term variation and the long-term *background* variation in order to discuss the evolution of the disk. In section 4, we try to interpret the long-term background variation of I_C by the disk precession of Hirata (2007). In the V/R long-term *background* variation, we show the possibility that the "V/R phenomenon" is triggered. The coexistence of short-term V/R variations in the periastron phenomenon and the "V/R phenomenon" in the long-term *background* variation is also touched upon.

¹ BeSS database (<http://basebe.obsppm.fr/basebe/>)

2. Data Selection

The data in the BeSS database consist of observations made with a variety of instruments (aperture diameter: 10 – 40 cm, long-slit spectrographs, echelle spectrographs, and various CCD detectors). These data have been already analysed by the group of observers introduced in section 1. The following points have been taken into account in order to deal with the long-term data again. For the study of long-term variations, it is desirable that the wavelength resolution R is constant, since measurements of the central intensity of the emission line profile, etc., can be obtained as a function of R . On the other hand, to increase the time resolution of the observation, it is necessary to select observations with a considerable range of R . To satisfy both these requirements, observations with R ranging from 10000 to 20000 were selected. In addition, it is required that the trend of changing profile intensity indicated by individual observations is relatively stable. As a result, a total of 520 observations were obtained. The average R -value distribution of the selected observations is mostly around 15000. Note that the R value follows the value described in the header of the downloaded fits file.

3. Analysis and Results

3.1. Measurement work

Each observed spectrum was normalised to the continuum light level (using Nijiboshi software²) and converted to the heliocentric wavelength system (use of IRAF). The processed spectra of individual observations can be downloaded from the personal website³.

The parameters for the intensity and radial velocity at three characteristic points of the normalised $H\alpha$ profile, i.e. the intensities I_{-B} , I_{-R} , radial velocities V_{r-B} , V_{r-R} at the blueward and redward emission peaks, and the intensity I_{-c} , radial velocity V_{r-c} at the central minimum, are calculated by the quadratic least squares fit to the above three points of the line. Note that the profile near the emission peak shows very complex variations, so we work with a small number of data points (about 10 – 20 data points) around the measurement point. Also, if the H_2O absorption components of the Earth's atmosphere are poorly mixed, the emission peak data are not measured (only the I_{-c} and V_{r-c} values are measured). The continuum of the $H\alpha$ emission line is estimated by interpolating from the continuum light level of the spectrum in the wavelength range widely sandwiched around the $H\alpha$ line (interpolation with a cubic spline function). Since the adjustment error of the continuum light is about $\pm 1\%$, the calculation error of the three intensity parameters of the emission line is about the same, reflecting the former, but the observation error of each observation data is quite large. Assuming that the observation date outside the period of periastron phenomena has a constant value, the empirical observation error at the emission peaks where atmospheric absorption tends to overlap to be δI_{-B} and $\delta I_{-R} = \pm 0.07$, and at the central minimum intensity is estimated to be $\delta I_{-c} = \pm 0.05$ (the magnitude of the error in

figure 1). Measurements separated by more than this error are considered reliable. Similarly, the empirical errors in radial velocity observations are δV_{r-B} and $\delta V_{r-R} = \pm 5 \text{ km s}^{-1}$ and $\delta V_{r-c} = \pm 5 \text{ km s}^{-1}$ (the magnitude of the error in figure 2). In addition, the errors in the emission line intensity ratio $V/R (= I_{-B} / I_{-R})$ and the mean emission peak radial velocity $V_{r-EP} = 0.5 \times (V_{r-B} + V_{r-R})$ derived from these measurements are empirically ± 0.02 , $\pm 3 \text{ km s}^{-1}$ (the magnitude of the error in figure 3).

3.2. Intensity parameters (I_{-B} , I_{-R} , I_{-c})

Figure 1 (top) shows the variation of the three intensity parameters for the blue and red emission peaks (I_{-B} , I_{-R}) and the central minimum (I_{-c}) from January 2009 to March 2023. The horizontal time scale is the heliocentric median time of the observation (header information of the spectrum) minus 245000. This horizontal time scale will be referred to simply as "T" in the following. The green vertical dashed line in the figure indicates when the companion becomes periastron, and the time is calculated according to the orbital parameter solution 3 of Nemravova et al. (2010). This is also the time when the radial velocity of the primary star due to orbital motion is almost minimal.

Figure 1 shows that the state of the variation discussed by Pollmann (2018, 2020) is reproduced. Also of interest is the rapid rise in I_{-c} above continuous light levels and the rapid increase in emission line peaks at the periastron phenomenon. During the period of $T = 9800 - 9900$, the observations for which the three data are not complete have the damage at the emission peaks due to the strong atmospheric H_2O absorption. Their emission peaks (I_{-B} , I_{-R}) were not measured. However, during the same period, there is a characteristic variation in the I_{-c} value, so they are specially displayed.

In January 2009, at the left end of the figure, according to Tanaka et al. (2007), the $H\alpha$ emission line component originating from the old disk disappeared, and only the emission from the new disk was observed. Thus, it can be said that the figure is an observational record of the evolution of the new disk. The figure appears to superimpose the short-term variations on top of the long-term *background* variation for the three parameters. It is clear that the onset of each short-term variation coincides approximately with the periastron time. Pollmann (2020) shows almost the same value as the orbital period of Pleione by Nemravova et al. (2010) from the periodic analysis of the I_{-c} value variations. Thus, repeated short-term variations are variations caused by the approach of the companion star to the disk of the primary star (periastron phenomenon). The long duration of the short-term variations suggests that the gravitational pull of the companion is inducing structural density changes in the disk.

3.2.1. Long-term background variation in I_{-c}

If we can separate the short-term variations, which periodically overlap in figure 1, from the long-term variations, it will be easier to understand the parameter changes in the figure. We first describe how to determine the long-term *background* variation of the I_{-c} value, which appears to be a simple change. Based on the distribution map of the I_{-c} value seen in the phase of the binary orbital period, and following the tracing of the $H\alpha$ profile time series, the periastron phenomenon of the short-

² Nijiboshi software (<http://yamanecoland.starfree.jp/nijibosi.html>)

³ personal website (<https://bessdata.yu-yake.com>)

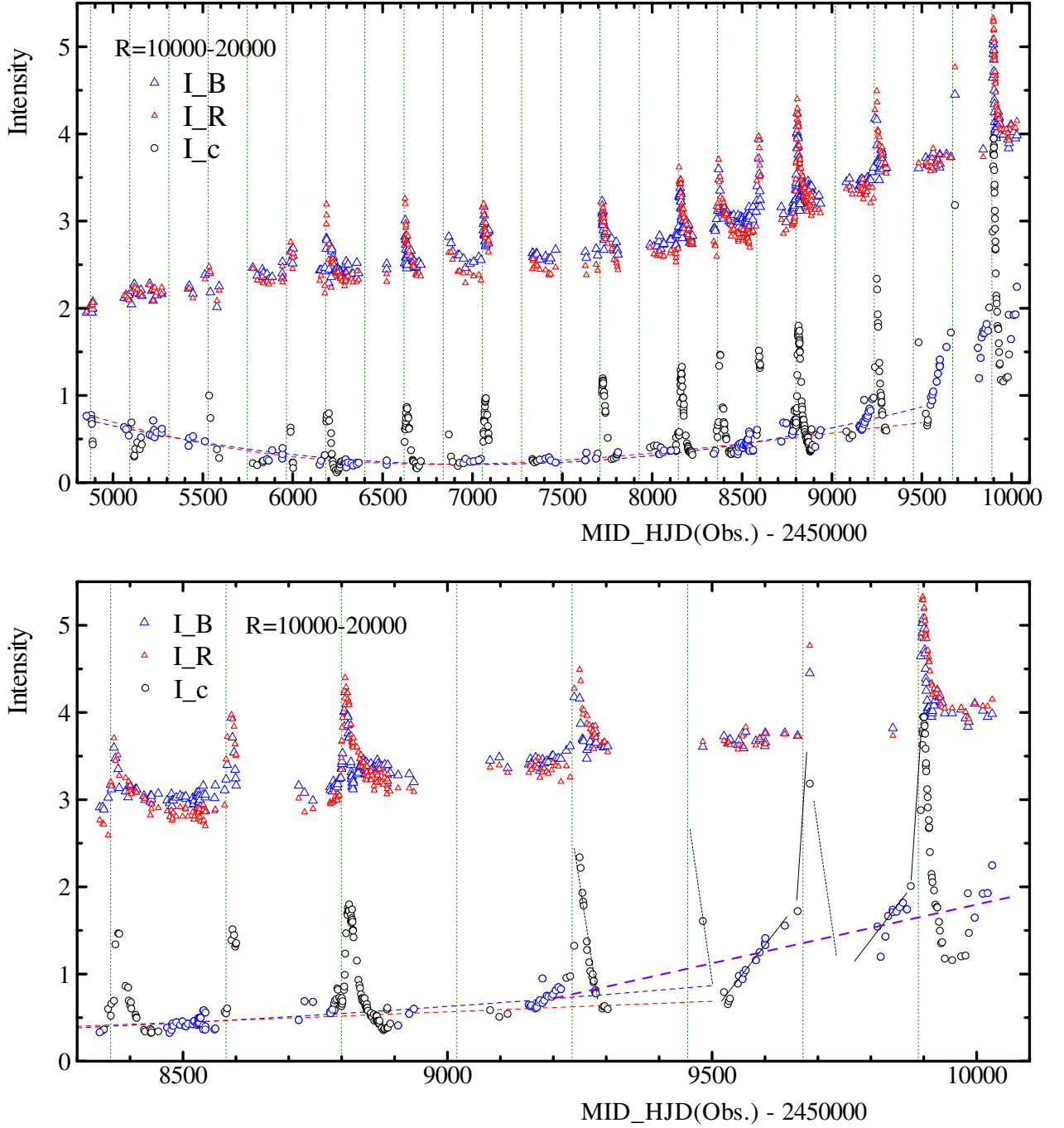


Fig. 1. Long-term intensity variation of the blue peak (I_B), red peak (I_R), and central minimum (I_c) of the $H\alpha$ double peak emission line. The horizontal scale subtracts 245000 from the heliocentric median time JD of observation. The green vertical dashed line indicates the periastron time of the companion star. In the sequence of " I_c ", data outside the periastron phenomenon are marked with blue circles. These data are fitted by the least squares method, and the result is plotted by the dashed lines, which is considered to be the long-term *background* variation. See the text for details. (Top) All data from January 2009 to March 2023. (Bottom) Enlargement after July 2018. After $T = 9000$ the pattern of the long-term *background* variation is tentatively highlighted by the dashed purple line.

term variation continues from about 15 days before periastron to 100 days after the periastron time (in the sequence of " I_{c} " in figure 1, data outside this period are marked with blue circles). In fact, this period is more than half of the binary orbital period of 218 days, but the stable I_{c} value continues outside this period (but, the range used is up to $T = 9000$). From this observational estimate, it can be assumed that the long-term *background* variation appears in the observed quantities during the period when the short-term variations disappear. The I_{c} values marked with blue circles show a trace of the long-term *background* variation. These points are fitted by the least squares method, and the results are shown in the figure by the blue dashed line (for the quadratic formula, correlation coefficient 0.90) and the red dashed line (for the cubic formula, correlation coefficient 0.91). The changes shown by the two curves are considered to be the long-term *background* variations of the I_{c} value between $T = 4800$ and $T = 9000$. The curves are extended to $T = 9500$ to compare the variation after $T = 9000$. The above approximation method for estimating the long-term *background* variation is only valid up to $T = 9000$ because it combines a small (visible to be stable) part of the long-term variation.

From the long-term *background* variation of I_{c} obtained, let's first consider the characteristics of the changes in the disk. It also provides a clue to consider the long-term variation of the emission line peak intensity in the figure. The resulting I_{c} long-term *background* variation curve (blue dashed line) starts to decrease from around $I_{c} = 0.72$, down to the minimum $I_{c} = 0.21$, and then starts to increase again, reaching $I_{c} = 0.63$. This variation gives the impression of almost symmetrical changes centred on the minimum. As $I_{c} < 1$ in the long-term *background* variation, the spectral phase due to the shape of the $H\alpha$ emission line is the Be-shell phase. The time of minimum in the I_{c} curve is estimated to be around $T = 7000$ (2014 – 2015). This epoch corresponds to the maximum shell activity in $H\alpha$.

Looking at the evolution of the emission peak intensity change in the period outside the periastron phenomenon (when the long-term *background* variation is visible) in figure 1, the emission intensity shows an upward trend. However, it should be noted that after the maximum of the shell activity at about $T = 7000$, the increase of the emission intensity stagnates for a while. This tendency may be due to the effect of the maximum shell activity.

The Fujii Bisei Observatory⁴ has published a long-term variation diagram of the equivalent width of the $H\beta$ line and of the metallic absorption equivalent width regionally summed over 600 Å in Pleione⁵. The maximum of metallic shell activity shown in the figure can be estimated to be about $T = 7300$ (2015 – 2016). The maximum of equivalent width of the $H\beta$ line also has the same epoch as the metal lines. This is similar to the estimate from the I_{c} variation of the $H\alpha$ emission

line, but it confirms that the timing of the maximum shell activity in the group of metallic absorption lines formed at the inner region of the disk is delayed by about one year from the $H\alpha$ line. Compared to Hirata's (1995) estimate of the maximum shell activity period 1981 based on the Fe II absorption equivalent width, the maximum period occurred about 34 years later. Again, the periodicity of the disk formation activity is suggested.

3.2.2. I_{c} variation after $T = 9000$

Figure 1 (bottom) is an enlarged view from $T = 8300$. After $T = 9000$, the state of the I_{c} short-term variations changes is very different from before. A different I_{c} variation appears than before. Furthermore, the stable period after short-term variations is not clear, and the I_{c} value always increases during its period. The thin black line superimposed on the figure is a curve tracing the I_{c} fluctuations, and the purple dashed line is a straight line connecting the observation data during the period when the short-term variations were thought to "disappear". In the figure, we have tried to highlight the feature that the pattern of the "long-term *background* I_{c} variation" changes after $T = 9000$. Around $T = 10000$, I_{c} shows always $I_{c} > 1$. In early March 2023, corresponding to the right end of figure 1, according to the $H\beta$ observation (échelle, $R = 9000$) in the BeSS database, the central absorption intensity of the $H\beta$ line increased and approached considerably the absorption intensity of the photospheric component. This is the time when the shell absorption component has become very weak. Such an I_{c} variation is an interesting observation, first observed at the turning point of the repeated phase transition of Pleione, the process of changing from the Be-shell phase to the Be phase. The Fujii Bisei Observatory has also published the long-term spectral variation of Pleione for the region $\lambda\lambda 4200 - 5600$ Å, normalised to the continuous light⁶. The two observations (January 2020 and September 2020) corresponding to the period around 9000 (just before the pattern of the long-term I_{c} variation changes) show that the metallic absorption lines are already weakening.

These changes in the $H\alpha$, $H\beta$, and metallic lines are very close to the observational guidelines for the onset of the Be phase of Pleione (see figure 1 of Rivinius et al. 2013). The March 2023 phase of Pleione is judged to be just before the phase transition to the Be phase. This is 35 years after the phase transition in the previous disk formation activity cycle (1988).

3.3. Radial velocity parameters (Vr_{-B} , Vr_{-R} , Vr_{-c})

Figure 2 (top) shows the evolution of the changes in the radial velocity parameters, the blue and red side emission peaks (Vr_{-B} , Vr_{-R}), and the central depth minimum (Vr_{-c}) for all observations. The values are converted to heliocentric radial velocities, not corrected for the orbital motion. Figure 2 (bottom) is an enlarged view after $T = 8300$. As in figure 1, the pattern of variation can be seen as the superposition of the short-term variations corresponding to periastron on the long-term *background* variation. We estimated the long-term *background* variation of Vr_{-c} , using the same method as for the

⁴ Fujii Bisei Observatory
(<http://otobs.sakura.ne.jp/FBO/index.html>).

Since 1996, the observatory has published a huge amount of low dispersion spectra ($R \sim 500$) focused on variable stars. The accumulation of observational data by fixed spectroscopic instruments is attractive.

⁵ 58th figure from the top in
(http://otobs.sakura.ne.jp/FBO/fko/gcas/bu_tau/bu_tau.htm)

⁶ 57th figure from the top in
(http://otobs.sakura.ne.jp/FBO/fko/gcas/bu_tau/bu_tau.htm)

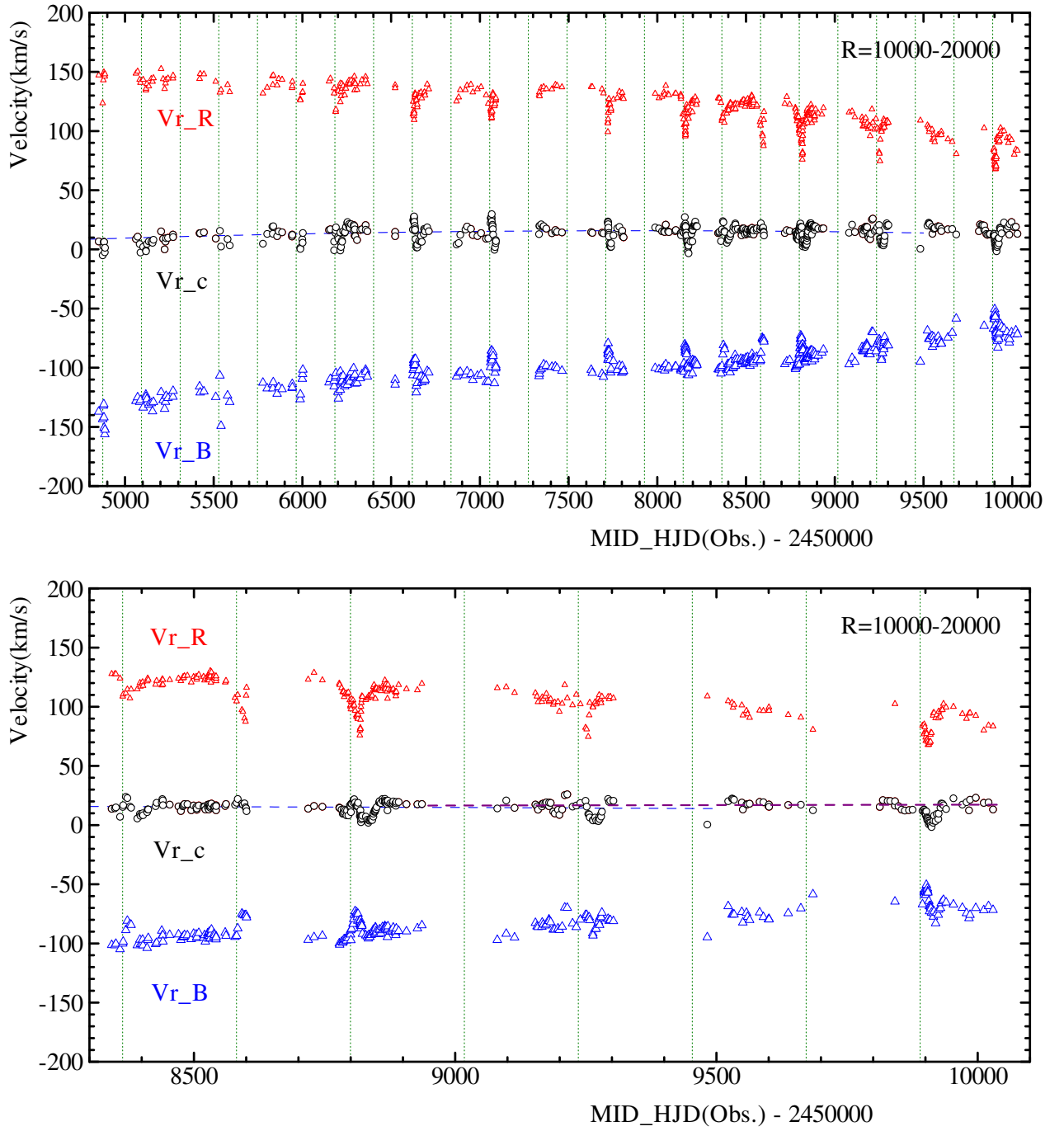


Fig. 2. Long-term variation of the radial velocities of the $H\alpha$ emission line, the blue emission peak Vr_B , the red emission peak Vr_R , and the central minimum Vr_c . The notation is the same as in figure 1, except that the vertical axis is the heliocentric radial velocity for the three velocities. In the Vr_c sequence the superimposed blue dashed line shows the long-term background variation, which is derived from the data outside the periastron phenomenon. (Top) All data from January 2009 to March 2023. (Bottom) Enlargement after July 2018. After $T = 9000$ the pattern of the long-term background variation is tentatively highlighted by the dashed purple line.

I_{c} variation. The result of the quadratic function fit (correlation coefficient is 0.53) is superimposed on the figure with a blue dashed line. According to Nemravava et al. (2010) figure 10, the radial velocity of the primary star's orbital motion can be regarded as almost constant during the period outside these short-term variations. The blue dashed curve reaches a maximum value of 15.8 km s^{-1} at about $T = 7800$, which is an increase of about 7 km s^{-1} compared to $T = 4800$. The long-term *background* Vr_{c} variation, which had a decreasing trend after the maximum, begins to show a new trend of increasing Vr_{c} values after $T = 9000$ towards $T = 10000$, when the spectral phase begins to shift to the Be phase (figure 2 (bottom), figure 3 (bottom)). The mean values of Vr_{c} (km s^{-1}) in the long-term *background* variation at some epochs around $T = 8500, 9180, 9840,$ and 10000 are $15.6 \pm 1.6(37), 16.5 \pm 4.6(18), 16.8 \pm 3.5(10),$ and $18.5 \pm 4.1(4)$. The error is the standard deviation and the number in parentheses is the number of observations. Although this change is within the range of observational error, it is likely to be related to the trend in I_{c} *background* variation in figure 1(bottom). Nemravova et al. (2010) figure 5 implies an increasing trend of Vr_{c} in the spectral phase transition from "Be-shell" to "Be" of the previous disk formation activity.

The emission peak separation PS ($= Vr_{R} - Vr_{B}$), read from the long-term *background* variation of Vr_{B} and Vr_{R} , gradually narrows even during the maximum period of shell activity. This change in PS is used to interpret the change in disk radius in "4. Discussion". However, the interpretation is based on a rough approximation that considers Pleione to be a single Be star once the periastron phenomenon of the companion subsides. During the periastron phenomenon the PS value shows a tendency to decrease rapidly, but the physical picture is not understood.

Short-term variations in radial velocity during periastron phenomena tend to be easy to read. First, Vr_{B} varies in an increasing direction, and Vr_{R} in a decreasing direction, and then returns to its original state. The variation of Vr_{c} seems to be related to the mean emission peak velocity Vr_{EP} ($= 0.5 \times (Vr_{B} + Vr_{R})$), i.e. it seems to be affected by the shift of the two side emission peaks (see figure 3). The binary orbital motion causes the radial velocity of the primary star to decrease by about 10 km s^{-1} before periastron and then to increase again (Nemravova et al. 2010). A plot corrected for orbital motion would also be necessary, but the trend of the figure does not change significantly.

3.4. V/R and radial velocity variation

Figure 3 (top) shows variations for V/R ($= I_{B}/I_{R}$), Vr_{EP} ($= 0.5 \times (Vr_{B} + Vr_{R})$) and Vr_{c} . Figure 3 (bottom) shows an enlarged view after $T = 8300$. To make it easier to read the long-term *background* variation of V/R, we have fitted the data from the period when the periastron phenomena did not occur using the least squares method. The result is shown as dashed lines (correlation coefficient 0.86). The value of the V/R in the *background* variation changes slowly in the order of " ~ 1 ", " > 1 ", " ~ 1 ", and " < 1 ". The maximum period of the V/R long-term *background* variation is about $T = 7800$, about two years after the maximum period of $H\alpha$ shell activity (about $T = 7000$) shown in figure 1. Note that as

the $H\alpha$ V/R reaches its maximum value, the $H\beta$ line begins to show $V/R < 1$ (Katahira et al. 2020), and as of March 2023, $V/R \ll 1$ (BeSS echelle spectrum).

To show the long-term *background* variation of the radial velocity, we use the long-term *background* variation of Vr_{c} , which is indicated by the dashed line and is already plotted in figure 2. Since the long-term *background* variations for the V/R and the radial velocity follow a similar pattern between $T = 4800$ and $T = 9000$, the correlation between them will be discussed later (see figure 5). Note that in the *background* variation after $T = 9000$ in figure 3 (bottom), Vr_{EP} shows a similar variation to the V/R (purple dashed line), but Vr_{c} is clearly different. There is a difference in the pattern of variation between Vr_{EP} and Vr_{c} in the *background* variation.

The V/R short-term variations that occur during the periastron phenomena show changes that are roughly similar to the radial velocity variations. However, the phase of the radial velocity change is slightly behind the V/R short-term variation, so the correlation does not appear. Although the $H\alpha$ profile variation diagram is not shown in this paper, the time variation of the profile shows a strangely "regular" sequential intensity change in the line during each periastron phenomenon. A detailed study of the shape change of the time series profile is necessary to understand the phenomenon.

4. Discussion

4.1. Interpretation of the long-term *background* variation of I_{c}

We wish to consider qualitatively the significance of the long-term *background* variation of the I_{c} value from the image of the Be disk model. Rivinius, Carciofi, and Martayan (2013) figure 1 shows the currently accepted disk model⁷. The change in profile shape due to the direction of the observer's line of sight (disk tilt) is shown with the profiles of a typical Be star. From such a disk model, in the Be-shell phase, Pleione is seen to be in the edge-on view. The particular state of $H\alpha$ central minimum intensity $I_{c} < 1$ in the Be-shell phase of Pleione is considered to be due to the high density of the disk (e.g. Hummel 1994; Iwamatsu & Hirata 2008; Silaj et al. 2014). Thus, the long-term *background* variation of I_{c} in figure 1 is thought to be indicative of the long-term variation that the disk exhibits around the edge-on state. We can consider two factors that determine the long-term *background* variation of I_{c} : disk density and inclination. It is a simplification to say that what causes the almost symmetrical variation in figure 1 is an increase or decrease in disk density, or a change in disk inclination.

Let's first take a look at the plots of the measurements relating to the disk density parameter. The long term *background* I_{c} variation shown in figure 1 (top) at $T = 4800 - 9000$ shows a symmetric trend with a minimum $I_{c} = 0.22$. Meanwhile, the emission line intensity is increasing. In figure 2 (top), the long-term variation of the emission peak separation

⁷ The Be disk is currently considered to be, (i) geometrically, the disk has a flat shape that spreads out on either side of the equatorial plane of the disk as one moves away from the central star, and (ii) physically, the disk is a viscous decretion disk formed by the supply of the angular momentum from the central star (Rivinius et al. 2013).

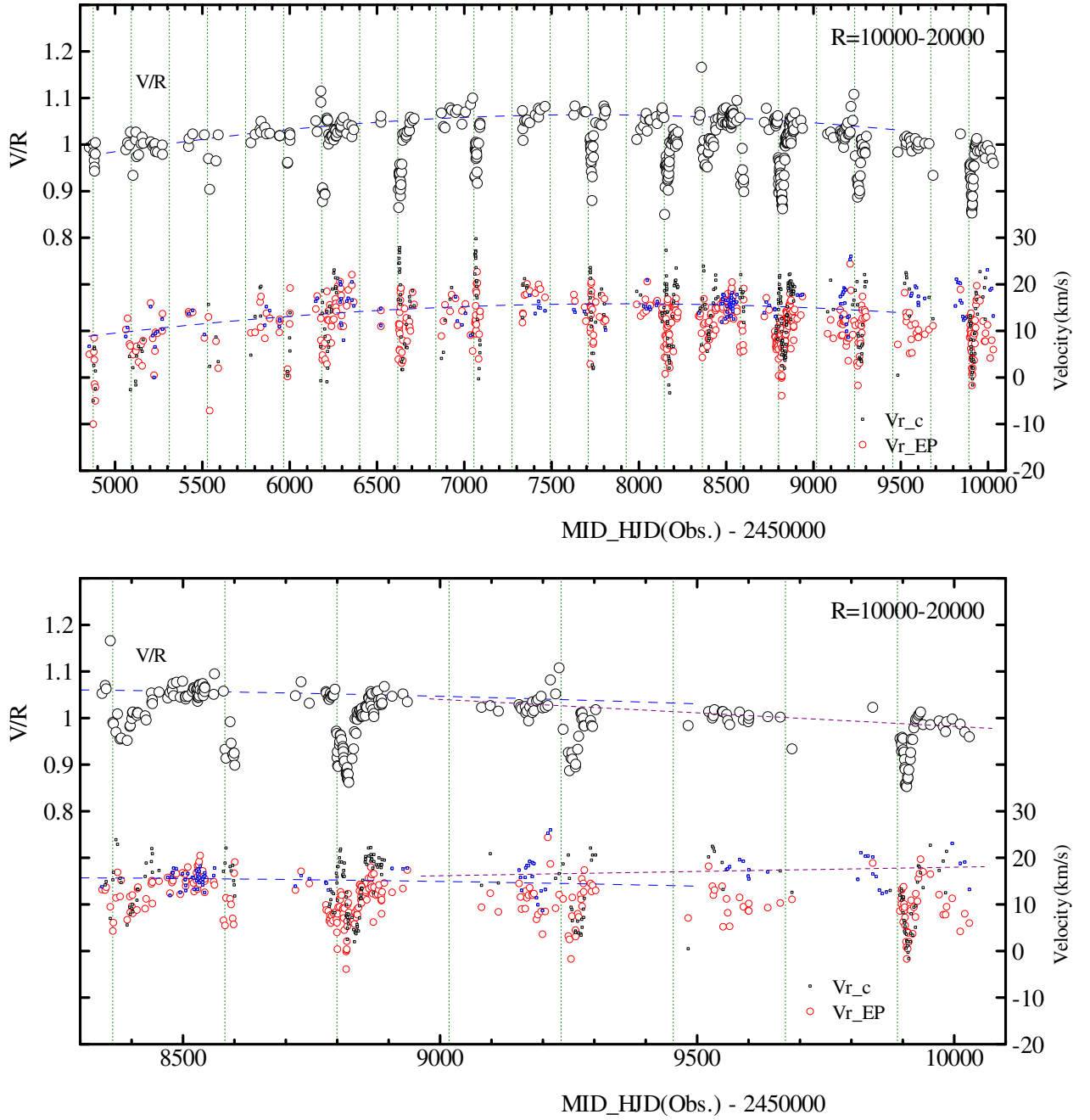


Fig. 3. Long-term variations of H α emission peak intensity ratio V/R , central minimum velocity V_{r_c} and mean emission peak velocity V_{r_EP} ($= (V_{r_B} + V_{r_R})/2$). The notation is the same as in figure 1, except that the left vertical axis is V/R , and the right vertical axis is the heliocentric radial velocity for V_{r_c} and V_{r_EP} . In the V/R sequence the superimposed dashed line shows the long-term *background* variation, which is derived from the data outside the periastron phenomenon. The same is done in the V_{r_c} sequence. In the V_{r_c} sequence the data outside the periastron phenomenon are represented by blue squares. (Top) All data from January 2009 to March 2023. (Bottom) Enlargement after July 2018. After $T = 9000$, the patterns of the long-term *background* variations for the V/R and V_{r_c} sequences are tentatively shown by the purple dashed lines.

PS ($= Vr_R - Vr_B$) shows a decreasing trend in the corresponding period. For a single Be star, a simple relationship between PS, disk inclination, and disk radius is considered (e.g. Hirata & Kogure 1977). It is an approximation that, for the same inclination, the disk radius increases as the PS decreases. Even taking into account the change in the inclination due to the precession of the disk, which will be discussed in the next section, it can be seen that the size of Pleione's disk continues to increase. Since the increase in the size of the disk can be interpreted as a result of the supply of gas from the central star to the disk, it is assumed that the density of the disk increases during this time. It is then difficult to generate a long term *background I_c* variation from up and down variations in the disk density.

The interpretation of the long-term *background* variation of *I_c* will be explained in the remaining "disk tilt". Here we use the image of the disk precession obtained by Hirata (2007) from the long-term polarization analysis of Pleione. Since the observations in the current disk formation period show similar changes to the previous disk formation period, so we assume that the same disk precession as in the previous period is occurring. Focusing the disk arrangement near edge-on, Hirata (2007) figure 3b, means that the disk gradually reaches the state of inclination $i = 90^\circ$ (at the edge-on) and then separates again to reach the state of $i = 60^\circ$ (at the early stage of the Be phase). This picture of the precession can roughly explain the present observation that the long-term *background* variation of *I_c* in figure 1 gradually reaches a minimum and then slowly increases again. Conversely, the long-term *background* variation of *I_c* in figure 1 can be used to claim that the precession of the disk has "reappeared".

As an extension of the above reasoning, the observation that the value of *I_c* is always $I_c > 1$ at about $T = 10000$ may indicate that the disk inclination is approaching $i = 60^\circ$. It is thought that the $H\alpha$ emission line profile for the Be phase begins to appear.

4.2. Intensification of the periastron phenomenon

The first confirmation of the periastron phenomenon seen in figure 1 is at the periastron time of $T = 4874$, according to the overlap of the periastron time and the fluctuation in which the *I_c* value decreases in the short-term variation. The next one is observed at $T = 5092$. After that, the short-term jump of the *I_c* value (correlated with the change of the emission peak intensity) can be used as a guide, making it easy to judge the periastron phenomenon. Looking at the "magnitude" of the jump, based on the curve of the long-term *I_c* *background* variation, it increases gradually towards the maximum period of shell activity and increases exponentially after the maximum period. This change clearly reflects the strengthening of the disk-companion gravitational interaction at periastron, as the disk radius increases and disk precession progresses.

Let's imagine a process where the interaction strengthens at an accelerating rate towards the transition to the Be phase. After $T = 8500$ in the middle, the narrowing of the emission peak separation PS in the long-term *background* variation seen in figure 2 is accelerated, and the disk radius is expected to increase rapidly. The increase in the disk radius seems to be the main reason for the increased interaction with the compan-

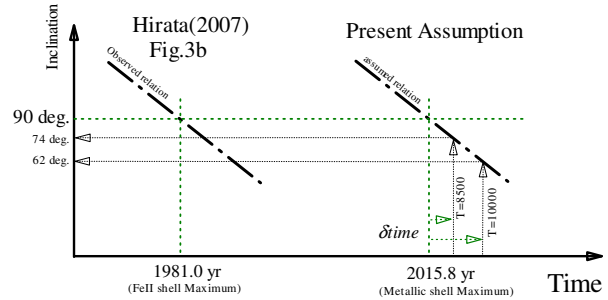


Fig. 4. Approximation for calculating the current disk inclination

ion star. When the disk radius is calculated using the variation pattern of the disk inclination from Hirata (2007), the increase in the radius at $T = 10000$ is about 1.7 times larger than that at $T = 8500$. It is quite possible that the increase in the disk radius contributes to the intensification of the periastron phenomenon. The present use of the inclination from Hirata (2007) is based on the time of the previous and current metallic shell activity maximum (1981.0, 2015.8 respectively). The converted inclination values are $i = 74^\circ$ for $T = 8500$ and $i = 62^\circ$ for $T = 10000$. This approximation process is illustrated by the hand-drawn figure (figure 4). This calculation also suggests that at the beginning of the Be phase, the current size of the disk may be larger than that of the previous disk formation activity (see Hirata 2007 figure 3c).

Since the periastron phenomenon begins to intensify after $T = 9000$ in spite of the gradual progress of the inclination change, the factor caused by the change in the 3-dimensional space arrangement may also be important. So let's consider the factors in the intensification due to the arrangement of the disk, whose inclination is approaching 60° due to the precession.

In the Hirata (2007) disk precession, the position of the disk changes as if it were perpendicular to the orbital plane of the companion star. And in the initial state of the Be phase, the tilt of the disk reaches $i = 60^\circ$. One of the factors that can be deduced from such a spatial configuration of the disk is that the light from the entire equatorial plane of the disk, where the periastron phenomenon can occur, reaches the observer more easily. In the period corresponding to the initial state of Be phase (January – February 1988), Doazan, Thomas, and Bourdonneau (1988) detected the appearance of superionized lines of C IV and Si IV, while the Fe II shell absorption components weakened in the UV. Hirata (2007) interpreted this detection of UV superionized lines as the appearance of the "stellar wind bellow and above the cool disk" due to the disk precession. Because of the change in inclination, we naturally assume that the disk has begun to show new, previously unseen regions, not only above the front face of the photosphere, but also around the photosphere. It is very possible that such a situation has already appeared by March 2023 during the current disk formation period. The intensification of the periastron phenomenon in question at around $T = 10000$ is thought to be an integral effect of "new areas" of the disk.

Another factor can be imagined as follows. Due to the precession, a change in the spatial configuration of the disk in the orbital plane of the companion star can create a situation

that intensifies the periastron phenomenon itself. This is because the gravitational interaction has an aspect that becomes stronger as the distance between the companion star and the disk decreases near the periastron. The sharp change in the I_c fluctuation shown on the right hand side of figure 1 could be the result of the change in the spatial configuration of the disk. Elucidating the factors involved in the intensification will clarify the interaction between the companion star and the disk.

During the intensification of the periastron phenomenon, we assume that the gas supply from the photosphere to the disk continues. The observation of 13 February 2020 in the BeSS database ($T = 8892$, $R = 5700$) shows that the broad and shell components of the Ca II K line weaken considerably. The intensity of this line is usually taken as a parameter indicating the degree of gas supply from the photosphere to the disk (Gulliver 1977). However, we believe that the weakening tendency of the Ca II K line corresponds to the weakening of the metallic shell absorption lines introduced in section 3.2.

4.3. Traces of the V/R phenomenon in the long-term background variation

The V/R phenomenon is the periodic V/R variation of the emission line profile that occurs in about 70% of Be-type stars (Mennickent & Vogt 1991). In the spectral type distribution, the number of stars decreases in the late type of B8 type, such as Pleione (Okazaki 1997). Pleione has also shown V/R phenomena during earlier periods of disk activity (Okazaki 1997; Hirata 2007). It has been shown theoretically that when the V/R phenomenon is observed, a stable one-armed density wave is activated in the Be disk and rotates in the disk (Okazaki 1996). If the intensity of the emission peak on the blue side of the profile is stronger than the intensity of the emission peak on the red side ($V/R > 1$), the whole profile shifts to the red side, and vice versa. Let's consider whether the V/R phenomenon, which shows such a correlation, also occurs during the current period of disk formation activity.

From figure 3 it can be seen that the long-term *background* variations of V/R and Vr_{EP} follow a similar pattern. Since the value of Vr_{EP} can be considered as roughly corresponding to the representative wavelength position of the profile, the correlation between the two parameters is plotted in figure 5 to check the existence of the V/R phenomenon. The marks plotted are data up to $T = 9000$ for the black marks, and data above $T = 9000$ for the red marks (the observation range for the *background* variation is not clearly found). We have the impression that the two sets are related over the whole V/R range. The figure means that the whole emission line shifts to the red side when $V/R > 1$, but starts to shift to the blue side when $V/R = 1$. Therefore, when all the data are fitted with a straight line using the method of least squares, a blue dashed line is obtained (correlation coefficient 0.53). A positive correlation is tentatively observed between V/R and Vr_{EP} .

For the first time since Pollmann and Vollmann (2014) pointed to the existence of the periastron phenomenon, we have identified traces of the so-called V/R phenomenon in the long-term *background* variation, a series of discrete data for the period outside the periastron phenomenon. However, after $T = 9000$ the selected data include data that cannot be visually judged to be in a state where the periastron phenomenon has

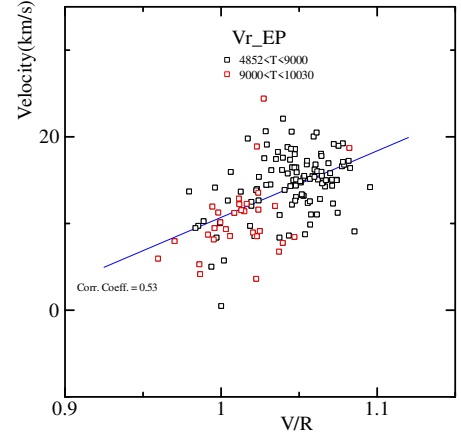


Fig. 5. Correlation diagram of V/R and Vr_{EP} . The data are for observation days considered to be out of the periastron phenomenon, and are color-coded by $T = 9000$.

subsided. Data with $V/R < 1$ are expected to be observed in the future, but it may be necessary to change the method of selecting data periods representing the long-term *background* variation from using I_c intensity to using emission line peak intensity.

Note that the correlation between V/R and $Vr(I_c)$ shows a scatter similar to the black squares in figure 5 up to the 9000 timescale, but the correlation disappears after $T = 9000$. The reason for this is that the variation pattern of the $Vr(I_c)$ is different from that of V/R after $T = 9000$, as shown in figure 3 (bottom).

4.4. Can the V/R phenomenon in the long-term background variation and the short-term V/R variation in the periastron coexist?

As can be seen in figure 1, the disk is gravitationally shaken with each periastron passage of the companion star. The V/R phenomenon in the long-term *background* variation shown in section 4.3 is only confirmed by connecting the data observed during the period when the periastron phenomenon seems to have subsided, so there is some uncertainty. However, let us dare to assume that the correlation diagram in figure 5 shows the appearance of the V/R phenomenon. Then the long-term *background* V/R phenomenon in the disk coexists with the short-term V/R variation during the periastron phenomenon. The variation of the V/R value in the periastron phenomenon shown in figure 3 is about twice as large as the variation considered in the long-term *background* variation in figure 5. Furthermore, in the $H\beta$ line formed in the inner region of the disk, the V/R variation synchronised with the $H\alpha$ line is observed during the periastron phenomenon (Katahira et al. 2020). This indicates that the gravitational influence of the companion extends into the inner region of the disk. The existence of the V/R phenomenon in the $H\alpha$ line means that the density wave is maintained throughout the disk, even though the periastron phenomenon occurs repeatedly and affects deep within the disk. It will be important to clarify whether the periastron phenomenon in the short-term variation and the V/R phenomenon in the long-term *background* varia-

tion really coexist.

Panoglou et al. (2018) simulated the $H\alpha$ line profile variations (V/R variations) produced by a double spiral density wave in the Be disk of a close binary system. Interestingly, they show something similar to the V/R variations that appear during the periastron phenomenon. This could be a clue to thinking about the periastron phenomenon.

5. Summary

The $H\alpha$ data of Pleione in the BeSS database are collective observations by amateur spectroscopic observers, providing the valuable high temporal resolution record. This paper uses 520 observations (wavelength resolution 10000 – 20000) in the database from January 2009 to March 2023. From the $H\alpha$ emission profile normalised to the continuous light level, we measured the intensities of the blue and red side emission peaks, the radial velocities at the peak intensities, the intensity of the central minimum between two emission peaks, and the radial velocity at the minimum. We have plotted the 14-year variation of the measured data for the above three characteristic points of the profile, and discussed the following:

- The 14-year variation is tentatively divided into the repeated short-term variations and the long-term *background* variation.
- The locus of the long-term *background* variation of the central minimum intensity may be a reflection of the disk precession.
- The V/R phenomenon may be occurring in the long-term *background* variation.

Acknowledgment

This work has made use of the BeSS database, operated at LESIA, Observatoire de Meudon, France, and the results of the long-term analysis of Pleione published by the Fujii Bisei Observatory. The author wishes to express his hearty thanks to the BeSS database and the Fujii Bisei Observatory. The author is grateful to the referee for the useful comments, which helped to improve the manuscript. Stimulated by the proof of the existence of the periastron phenomenon by Pollmann and Vollmann (2014), I started to study the data of Pleione in the BeSS database with the help of Drs. R. Hirata (ex-Kyoto University) and S. Honda (University of Hyogo). I learned a great deal from the discussions with both of them at that time. I am deeply grateful to both of them.

References

- Doazan, V., Thomas, R. N., & Bourdonneau, B. 1988, A&A, 205, L11
 Gies, D. R., McKibben, W. P., Kelton, P. W., Opal, C. B., & Sawyer, S. 1990, AJ, 100, 1601
 Gulliver, A. F. 1977, ApJS, 35, 441
 Hirata, R. 1995, PASJ, 47, 195
 Hirata, R. 2007, in ASP Conf. Ser., 361, Active OB-Stars: Laboratories for Stellare and Circumstellar Physics, ed. S. Stefl et al., San Francisco: ASP, 267
 Hirata, R., & Kogure, T. 1977, PASJ, 29, 477
 Hummel, W. 1994, A&A, 289, 458

- Iwamatsu, T., & Hirata, R. 2008, PASJ, 60, 749
 Katahira, J., Hirata, R., Ito, M., Katoh, M., Ballereau, D., & Chauville, J. 1996, PASJ, 48, 317
 Katahira, J., Maeno, S., Honda, S., & Charbonnel, S. 2020, 第 25 回天体スペクトル研究会集録, 28
 McAlister, H. A., Hartkopf, W. I., Sowell, J. R., Dombrowski, E. G., & Franz, O. G. 1989, AJ, 97, 510
 Mennickent, R. E., & Vogt, N. 1991, A&A, 241, 159
 Nemravová, J., et al. 2010, A&A, 516, 80
 Okazaki, A. T. 1996, PASJ, 48, 305
 Okazaki, A. T. 1997, A&A, 318, 548
 Panoglou, D., Faes, D. M., Carciofi, A. C., Okazaki, A. T., Baade, D., Rivinius, T., & Borges Fernandes, M. 2018, MNRAS, 473, 3039
 Pollmann, E. 2018, IBVS, 63, 6239
 Pollmann, E. 2020, BAVSR, 69, 81
 Pollmann, E., & Vollmann, W. 2014, BAVSR, 63, 149
 Rivinius, T., Carciofi, A.C., & Martayan, C. 2013, A&A Rev., 21, 69
 Roberts, L. C. Jr., Turner, N. H., & ten Brummelaar, T. A. 2007, AJ, 133, 545
 Silaj, J., Jones, C. E., Sigut, T. A. A., & Tycner, C. 2014, ApJ, 795, 82
 Tanaka, K., Sadakane, K., Narusawa, S.-Y., Naito, H., Kambe, E., Katahira, J.-I., & Hirata, R. 2007, PASJ, 59, L35
 Taranova, O., Shenavrin, V., & Nadjip, A. D. 2008, Peremennye Zvezdy Prilozhenie, 8, 6